JACS
JOURNAL OF THE AMERICAN CHEMICAL SOCIETY

Article

pubs.acs.org/JACS

Mapping Intracellular Diffusion Distribution Using Single Quantum Dot Tracking: Compartmentalized Diffusion Defined by Endoplasmic Reticulum

Hui Li, Shuo-Xing Dou, Yu-Ru Liu, Wei Li, Ping Xie, Wei-Chi Wang, and Peng-Ye Wang*

Key Laboratory of Soft Matter Physics, Beijing National Laboratory for Condensed Matter Physics, Institute of Physics, Chinese Academy of Sciences, Beijing 100190, China

W *Web-Enhanced Feature* *S* *Supporting Information*

ABSTRACT: The crowded intracellular environment influences the diffusion-mediated cellular processes, such as metabolism, signaling, and transport. The hindered diffusion of macromolecules in heterogeneous cytoplasm has been studied over years, but the detailed diffusion distribution and its origin still remain unclear. Here, we introduce a novel method to map rapidly the diffusion distribution in single cells based on single-particle tracking (SPT) of quantum dots (QDs). The diffusion map reveals the heterogeneous intracellular environment and, more importantly, an unreported compartmentalization of QD diffusions in cytoplasm. Simultaneous observations of QD motion and green fluorescent protein-tagged endoplasmic reticulum (ER) dynamics provide direct evidence that the compartmentalization results from micron-scale domains defined by ER tubules, and ER cisternae form perinuclear areas that restrict QDs to enter. The same phenomenon was observed using fluorescein isothiocyanate-dextrans, further confirming the compartmentalized diffusion. These results shed new light on the diffusive movements of macromolecules in the cell, and the mapping of intracellular diffusion distribution may be used to develop strategies for nanoparticle-based drug deliveries and therapeutics.

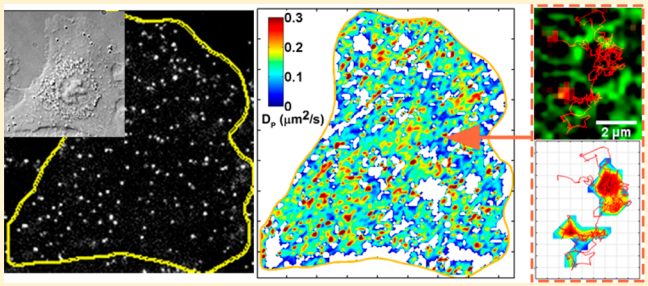

INTRODUCTION

The intracellular environment is crowded with small solutes, macromolecules, and different kinds of organelles. Intracellular protein diffusion depends not only on the fluid-phase viscosity of the cytoplasm but also greatly on collisions with macromolecules and organelles.[1−5] The mobility of proteins is critical for their interactions and functions, and many efforts on its measurements have been reported over the past two decades, showing significantly slower diffusion for protein-sized macromolecules in cytoplasm than in pure water.[6,7] Fluorescence recovery after photobleaching (FRAP) and fluorescence correlation spectroscopy (FSC) have been extensively used for diffusion measurements, by monitoring the fluorescence signal at a fixed area of the cell defined by the laser spot.[6,8−10] The results thus obtained point by point, however, are spatially and temporally averaged and cannot well describe the heterogeneous environment in the cell.[1,11]

The SPT method with fluorescent probes allows for reconstructions of single-molecule trajectories with nanometer spatial and millisecond temporal resolutions.[12,13] Unlike FRAP and FCS, SPT can provide direct information about individual particles and identify complex and heterogeneous environments according to the dynamics of particle motions.[2,8] In fact, SPT has already become the preferred choice in investigating the spatial organizations of membranes and the lateral diffusion of membrane proteins.[14−16] It reveals that membranes contain nanometer-scale compartments that restrict lateral diffusion of proteins.[17−19]

In single cells, however, the precise diffusion distribution of macromolecules as well as the relevant intracellular environment at the nanometer level remain to be studied. The method of particle-tracking microrheology may be employed to study the viscoelastic properties of the cytoplasm[20] but is not applicable to intracellular diffusion measurements because of the large probing beads (>100 nm) used. Recently, semiconductor QD probes become the potential tools in SPT studies. As QDs have superior brightness and photostability compared with conventional fluoresce dyes and smaller size than beads, they are the ideal probes for measuring the intracellular diffusion.[21,22] Nevertheless, how to deliver QDs into the cytoplasm and avoid their nonspecific binding are still not well resolved. The current nanoparticle-delivering approaches, including cell penetrating peptides, polymer-mediated, and electroporation methods, often cause probes to be trapped in the endocytic pathway or form aggregates in the cytoplasm.[23,24] Microinjection or ballistic injection has a better performance, but they are physically destructive for cells.[20,23]

Here we use a cell-loading technique to overcome the above problems and develop a novel method to map rapidly the

Received: November 3, 2014
Published: December 23, 2014

DOI: 10.1021/ja511273c
J. Am. Chem. Soc. 2015, 137, 436−444

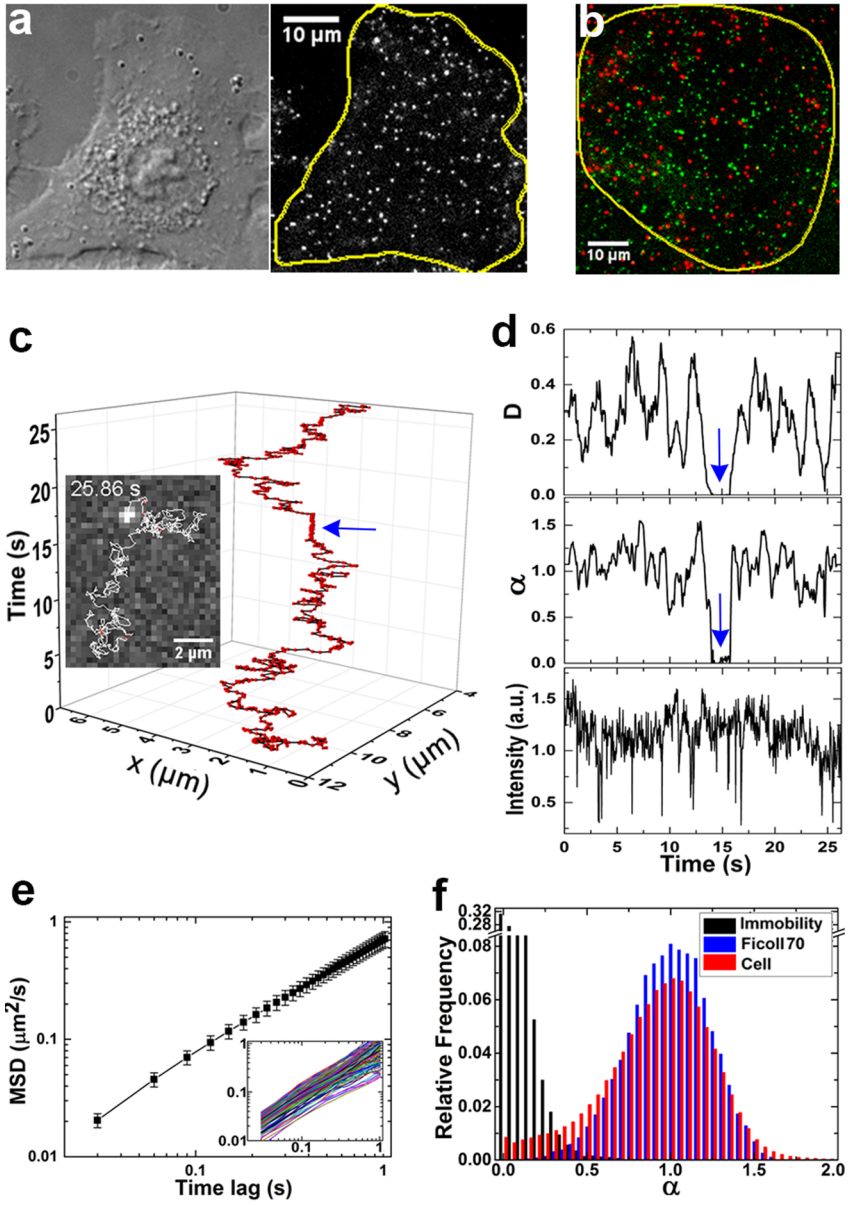

Figure 1. Delivering QDs into A549 cells and tracking individual QDs for measuring the diffusion coefficients. (a) DIC (left panel) and fluorescence (right panel) images of a A549 cell. QD655-streptavidin at a concentration of 5 nM was delivered into the cell through a pinocytic process. The cell morphology maintained normal and QDs dispersed homogeneously in cytoplasm at the focus plane near the glass. The cell boundary is marked by a yellow line. (b) Fluorescence image of a A549 cell, into which QD655- and QD525-streptavidin were delivered together. (c) Position of a single QD as a function of time, with a temporal resolution of 30 ms. The arrow indicates a segment of immobilization. Inset, the corresponding fluorescence image of the QD with its path marked by white lines. (d) The diffusion coefficient D, exponent α, and intensity versus time for the QD trajectory in (c). Arrows indicate the period of immobilization. The window size for local MSD analysis is 30 points. (e) Averaged whole MSD of QD655-streptavidin (in 23 A549 cells) as a function of lag time (<1 s) has an exponent α of ~0.92. Inset, randomly selected samples (100) of MSD curves. (f) Distributions of temporal exponent α of the QDs, when they were immobilized on glass (= 0.10 ± 0.09, n = 106717), diffusing in Ficoll 70 (30 wt %) (= 0.98 ± 0.25, n = 86642), or in cells (= 0.91 ± 0.32, n = 238683). QDs in Ficoll 70 were considered as in Brownian diffusion. The motionless QDs (with overall displacement <100 nm in 1 min imaging) in cells were removed prior to the statistics.

intracellular diffusion distribution by combing SPT and QDs. We provide direct evidence that endoplasmic reticulum (ER) tubules compartmentalize the QD diffusion and ER cisternae form diffusion-restricted perinuclear areas.

RESULTS AND DISCUSSION

QDs were first internalized in the cytoplasm of cultured A549 cells (human lung carcinoma) with a cell-loading technique based on the osmotic lysis of pinocytic vesicles (Figure 1a and Movie 1).[25] This technique is more rapid and simpler than microinjection, without obvious altering of normal cell morphology and functions. More importantly, we have found that the internalized QDs are the suitable probes to detect intracellular diffusion environment using SPT: (i) QDs were individually dispersed, without being trapped in the endocytic pathway or vesicles, as was demonstrated by the non-colocalization of QD655- and QD525-streptavidin loaded together (Figure 1b); (ii) the diffusion coefficient of QDs measured with SPT was inversely proportional to the macroscopic solution viscosity (Figure S1);[26] and (iii) the

DOI: 10.1021/ja511273c
J. Am. Chem. Soc. 2015, 137, 436−444

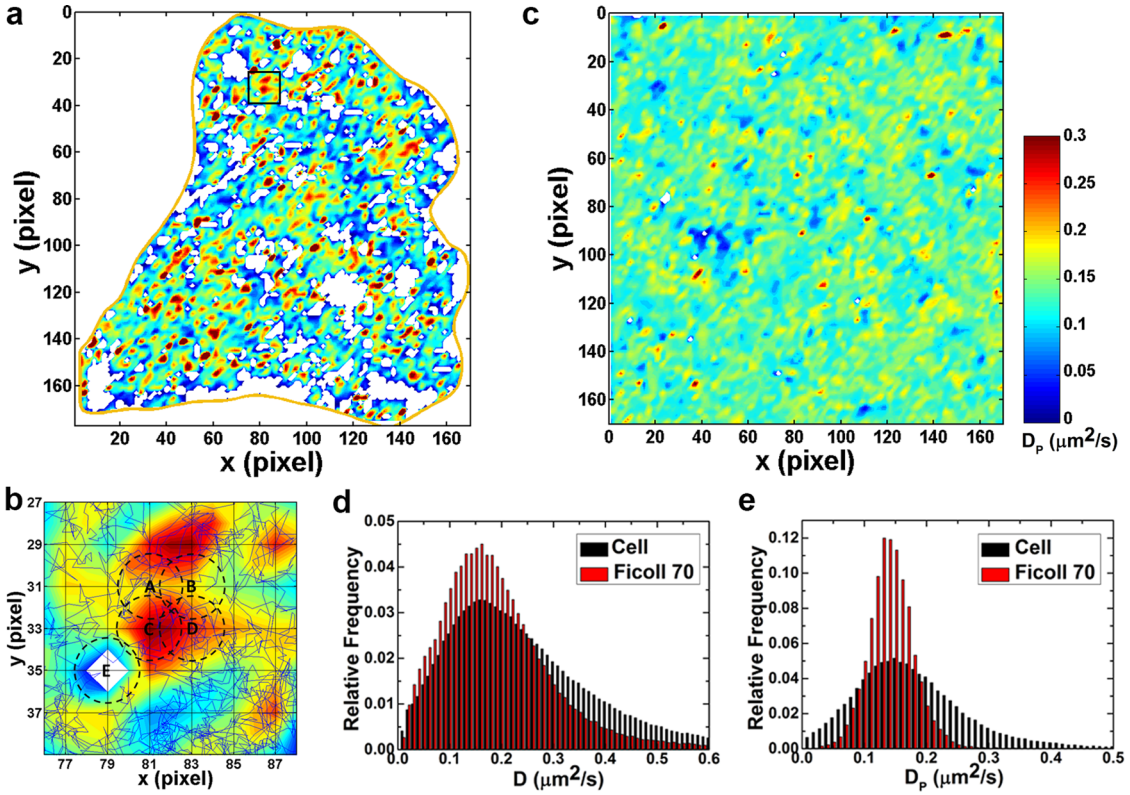

Figure 2. Mapping of the diffusion distribution of QD655-streptavidin in a single cell. (a) Diffusion map for the A549 cell in Figure 1a. The color from blue to red correspond to D_P (local diffusion coefficient) from 0 to 0.3 $\mu m^2/s$. (b) Magnified image of the rectangular part marked in (a) to illustrate the method for plotting the diffusion map. The four points A, B, C, and D are four grid nodes with 2-pixel spacing. The D_P at each point is calculated using the trajectory segments within the circular region of 1.5 pixel radius around the point. The blank area at point E is because of insufficient trajectory segments within the cycle around this point for D_P calculation. For a valid point of D_P, each of the first three lag times of MSD curve must be calculated using more than five samples. The diffusion map was then plotted in Matlab with a built-in smoothing process. The diffusion map corresponding to (a) without the smoothing process is shown in Figure S5. (c) The diffusion map for Ficoll 70 (35 wt %). In (a) and (c), the averaged sample number for determining each of the first three points of MSD curve was over 40. (d) Probability distributions of diffusion coefficient for each point along all the trajectories, D, in cells and Ficoll 70 (35 wt %), with mean values of 0.24 and 0.19 $\mu m^2/s$, respectively. The number of QD trajectories used for the statistics are ~28,200 (in 23 cells) and 13,060 (10 experiments), respectively. (e) Probability distributions of local diffusion coefficient at grid nodes in the diffusion maps, D_P, in cells and Ficoll 70 (35 wt %). The number of maps used for the statistics are 23 and 10, respectively.

nonspecific binding of QDs to intracellular molecules is insensitive to the QD dimensions. This was demonstrated by the quite similar relative diffusion rates, D_{QD655}/D_{QD525}, in Ficoll 70 (30 wt %) (0.87) and in A549 cells (0.89) (Figure S2 and Table S1), which suggests the ratio of Stokes radii of the two QDs remains basically unchanged, implying the strength of nonspecific interactions between the two QDs and the cytoplasm is of the same magnitude. Actually, according to previous studies by Liße et al.,[27] the QD655- or QD525-streptavidin should have greatly reduced nonspecific interactions with the cytoplasm due to the heavy PEG surface coating. The amount of internalized QDs in single cells was also determined quantitatively (Figure S3).

Normally, we used a 5 nM delivering QD concentration to ensure sufficient amount of QDs being internalized and acquired 33 Hz continuous imaging in 1 min for further analysis. Figure 1c shows a typical QD movement trajectory, consisting of mainly diffusion with occasional immobilization. To identify the heterogeneity of the environment, we used a local MSD window algorithm to obtain the dynamic parameters along a trajectory (Figure 1d and see Experimental Section for details).[12,28] The values of the exponent α and diffusion coefficient D fluctuate around the mean values except for the time duration of immobilization, indicating the environment diversity. Note that the fluorescence intermittency (blinking) demonstrates the QD was individual (Figure 1d).[22] The averaged whole MSD curve for short lag time (<1 s) of QDs from 23 cells has $\alpha = 0.92$ (Figure 1e), suggesting the motions of QDs are subdiffusive.[2,12] By comparing the α distributions with the control experiments for QDs in Brownian motion and stationary state, the temporal immobilization of QDs in cells was identified (Figure 1f). For the immobile events, our method gave the same results as the positional accuracy measurement (Figure S4). We will only select the trajectory segments with $0.5 < \alpha < 1.5$ for further diffusion statistic analyses, discarding the few stationary ($\alpha < 0.5$) as well as active transport ones ($\alpha > 1.5$).

We further tested the effect of surface modification on QD diffusion (Table S1) and then selected the QD655-streptavidin for the following experiments. The diameter of QD655-streptavidin is determined to be 27 nm (Figure S1), and its mean diffusion coefficient in A549 is 0.24 $\mu m^2/s$, consistent with those reported for macromolecules of comparable sizes measured by ensemble-averaged methods.[1] This D value is nearly 70-fold smaller than that in aqueous solution ($D_0 = 16.5$ $\mu m^2/s$), due to the molecular crowding in cytoplasm, and the

DOI: 10.1021/ja511273c
J. Am. Chem. Soc. 2015, 137, 436−444

ratio D/D_0 lies within the detected range, 0.001−0.5, for macromolecules.[1] Besides, it should be noted that other previous studies have also reported that D/D_0 is around 0.1−0.2 using the FRAP and FCS methods,[10,27,29,30] which is probably due to several factors: (i) The apparent Stokes radii of diffusing QDs may increase because of the inevitable nonspecific interaction, by acquisition of a protein corona or transient binding to intracellular structures; (ii) in the anisotropic environment in cells, the SPT performed in 2D from the projection of 3D movements, probably underestimates the diffusion rate compared with the FRAP[10,29] and FCS[27,30] in 3D; and (iii) the different time resolutions of the measurements between the FRAP[29] and FCS[27,30] apparatuses (microsecond resolutions, about 1 μs/frame) and the SPT we used (millisecond resolution, 30 ms/frame). Because the probe motion in cells is subdiffusive (with a downward curvature in MSD plots), the measured D would decrease with increasing observation time interval. This phenomenon is also observed on cell surface.[31] In addition, we have measured the mean D for the noninteraction probe fluorescein isothiocyanate (FITC)-dextran in cells and obtained a value of 0.56 $\mu m^2/s$, which is also lower than 1−2.5 $\mu m^2/s$ as measured by FRAP,[10,29] supporting the above points (ii) and (iii).

The diversity of the dynamic parameters of QDs results from the intracellular heterogeneous environment. Since SPT provides the direct information about locations where individual QDs diffuse, we are able to map the intracellular diffusion distribution (Figure 2a). The cell was divided into square grids, and the local diffusion coefficient at each grid node was calculated using the segments of trajectories within a circular region centered at the node (Figure 2b). The grid size (or spatial resolution) is 2 pixels (533 nm), and the radius of the circular region is 1.5 pixels (400 nm), which are chosen by considering the QD diffusion rate and sample sizes (see Experimental Section for details). In the diffusion map, there are many high diffusion rate areas surrounded by restricted diffusion and blank areas, demonstrating the heterogeneous and compartmentalized diffusion behaviors of QDs. Blank areas here correspond to regions where QD trajectories are not sufficient for calculation or there is no QD at all. To verify the accuracy of the diffusion map, freely diffusing QDs in viscose Ficoll 70 (35 wt %) were imaged and analyzed under the same experimental conditions. In this case, a much more homogeneous diffusion map was obtained (Figure 2c), with fluctuations obviously lower than that in the cell (see Figure 2e). It should be noted that small fluctuations in the diffusion map for Ficoll 70 were inevitable because of the limitation of data sampling with 1 min imaging. Furthermore, we compared the distributions of diffusion coefficients for each point along trajectories (D) and those at all points (D_P) in the diffusion maps. Although the distribution of D in Ficoll 70 (35 wt %) is similar to that in the cell (Figure 2d), the D_P in Ficoll 70 has obviously a narrower distribution than that in the cell (Figure 2e). In other words, the random fluctuations of D (this is the main source of D variation in the case of Ficoll 70) are partially averaged out in obtaining the diffusion maps by calculating D_P, while the variations of D caused by intracellular heterogeneity are preserved. This confirms that the diffusion map have effectively revealed the heterogeneous environment in living cells.

To have volume diffusion maps of the whole cell, we studied the QD diffusion at different sections of a cell (Figure 3a and Movie S2). The first layer, which is nearby the adherent cell surface, and the fourth layer, which is beneath the apical cell surface, have diffusion maps similar to that in Figure 2a. The second and third layers, however, exhibit two distinct diffusion regions, a diffusion-restricted region surrounded by a normal heterogeneous diffusion region. The restricted region is larger than the cross section of the nucleus, and only few QDs have entered into it. This is consistent with the perinuclear size-excluding area found previously,[32] though its origin remains unclear up to now. The average diffusion rate in the restricted region is much lower than that in the normal regions (Figure 3b). The MSD curve also illustrates the difference in diffusion

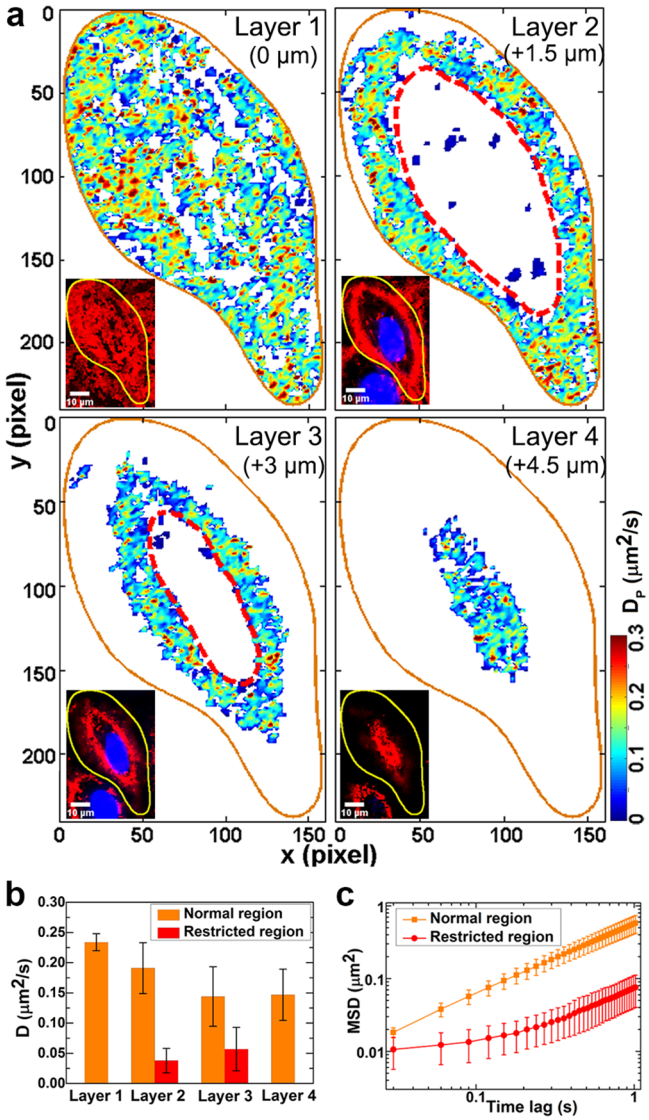

Figure 3. Diffusion maps of different layers in a single cell. (a) The A549 cell was imaged at four different layers successively to cover the entire diffusion distribution of QD655-streptavidin in the cell. Layer 1 is near the glass surface, and layers 2−4 are 1.5, 3, and 4.5 μm away from the glass surface, respectively. The cell boundary (yellow line) is determined at the first layer with bright-field cell imaging. The diffusion-restricted regions are marked by dashed lines. Inset, superimposed images of 2000 consecutive frames of QDs (red) overlaid with the image of nucleus (blue). (b) Average diffusion coefficients in the normal and diffusion-restricted regions in the four layers. (c) Plots of average MSD in the two regions in the second layer. Images of four cells were used for the data in (b) and (c).

DOI: 10.1021/ja511273c
J. Am. Chem. Soc. 2015, 137, 436−444

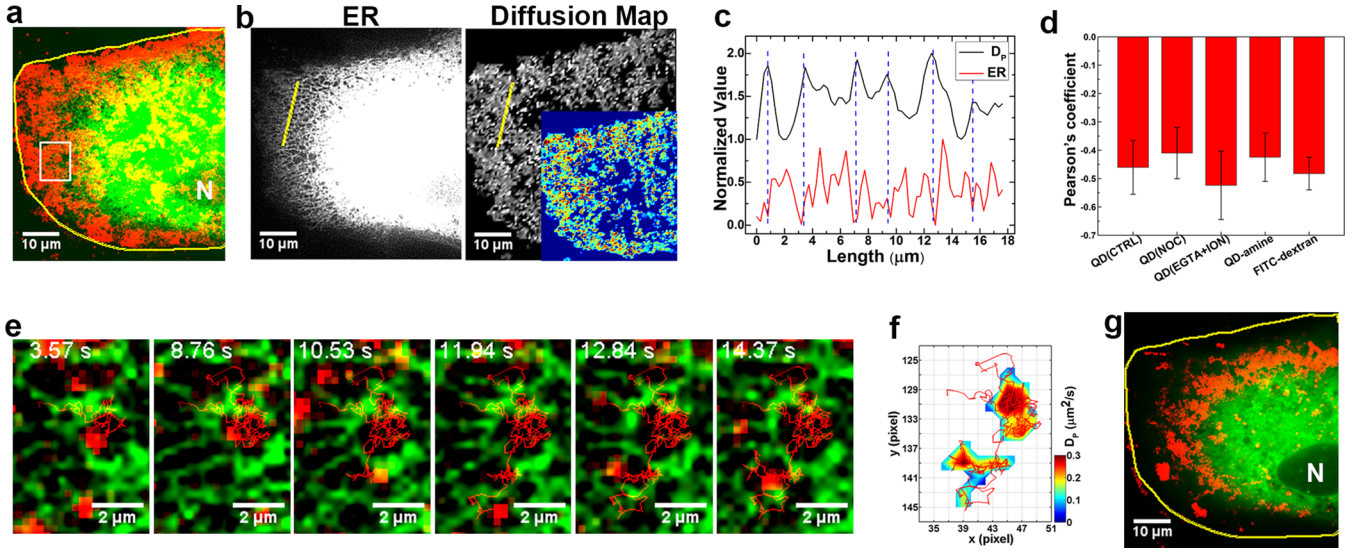

Figure 4. ER compartmentalizes the QD diffusion in the cells. (a) Merged image of GFP-ER (green) with the superimposed image of 2000 consecutive frames of QDs (red) in the first layer of a A549 cell, showing the good overlap of the ER and the QD trajectories. (b) The ER fluorescence image and the diffusion map are transformed into gray-scale images for quantitative comparison. Inset, the colorized diffusion map with all the blank areas colored in dark blue before transformation. The ER image used was the middle one in the image series of 1 min. (c) Negative correlation between the ER fluorescence intensity and the D_P of diffusion map along the same line indicated in (b). The two gray-value curves are normalized to the range of 0−1. For clarity, the D_P curve is displaced upward. (d) The PCs for the ER fluorescence intensity and the D_P of diffusion map for QD655-streptavidin in control cells (CTRL, $n = 12$, $p = 0.04$), in nocodazole-treated cells (NOC, $n = 7$, $p = 0.04$), in EGTA and ionomycin-treated cells (EGTA+ION, $n = 9$, $p = 0.01$), for QD655-amine in control cells ($n = 7$, $p = 0.04$) and for FITC-dextran (500 kDa) in control cells ($n = 8$, $p = 0.03$). All the results are from more than three cells. (e) Image series of a QD trajectory (red) overlaid with GFP-ER (green) in the rectangular region marked in (a). The ER morphology changed with time. (f) Diffusion map plotted using the trajectory in (e). (g) Merged image of GFP-ER (green) with the superimposed image of 2000 consecutive frames of QDs (red) in the second layer. The perinulear ER cisternae are sheet-like structures that are not spatially resolved here. The cell boundary is marked by a yellow line, and the nucleus position is denoted by N.

manner in the two regions (Figure 3c). Clearly, there exist a perinuclear barrier that restricts seriously QD diffusion.

The spatial-resolved diffusion maps of the single cells revealed a previously undetected compartmentalized diffusion. In the following, to investigate the origins of the heterogeneous diffusion map and the perinuclear barrier observed above, we thus carried out studies on the possible effects of several cellular organelles. The compartmentalized diffusion was present in the whole first layer, suggesting that some abundant and widespread organelles, such as cytoskeletons and ER, may play the major role. Note that the mitochondria are ruled out because they are located mainly in the perinuclear region (Figure S6). So we treated the cells with nocodazole to depolymerize microtubules (Figure S7a), cytochalasin D to depolymerize actin filaments (Figure S7b), and ionomycin (a calcium carrier) to fragment and produce disconnected ER elements (see following images for ionomycin effect).[33] We found the mean diffusion coefficient for QD655-streptavidin is decreased by <10% in microtubule- or actin-depolymerized cells, whereas it is markedly increased by ∼80% in ER-fragmented cells (Table S1). Similar results were obtained with QD655-amine. ER is a continuous membrane system consisting of nuclear envelope, sheet-like cisternae and an interconnected tubular network.[34] Our results suggest that the ER network may be mainly responsible for the highly restricted QD diffusion.

We next transfected cells with green fluorescent protein (GFP)-ER and used the two-color living-cell imaging technique to simultaneously track the QD and GFP-ER movements. The interconnected tubular net of ER extended ubiquitously into the cell periphery where QDs diffused (Figure 4a,b). Interestingly, D_P in the diffusion map and ER intensity in the fluorescence image along a given line show a markedly negative correlation (Figure 4b,c): the peak points of D_P coincide with minimum points of ER intensity. To further quantify the correlation, we used the Pearson's coefficient (PC).[35] Theoretically, PC ranges from 1 to −1, with 1 indicating complete positive correlation, −1 complete negative correlation, and zero no correlation, respectively. The mean PC for the ER fluorescence intensity and the D_P of diffusion map is −0.46 ± 0.09 (Figure 4d), consistent with a negative correlation. This indicates that ER tubules define micron-sized domains that compartmentalize QD diffusion. Note that one possible reason for the deviation of PC from −1 is that the ER network was continuously reorganizing, thus increasing the data noise. Figure 4e shows a typical trajectory of a QD making compartmentalized diffusion nearby dynamic ER tubules (Movie S3). The QD diffused in a micron domain formed by ER tubules for several seconds, until it escaped and entered another one. The two separate areas in the diffusion map plotted using this trajectory overlap well with the two micron domains (Figure 4f). In the second layer, the ER formed sheet-like cisternae in the perinuclear region that restricted QD diffusion (Figure 4g), just as in the case of Figure 3. The few QDs in this region underwent slow movements together with the ER cisternae.

The ER structure is known to form along the microtubule network.[36] To rule out the possible role of microtubule in the compartmentalized diffusion, we performed a control experiment with nocodazole-treated cells. The experiment condition for disrupting the microtubule architecture was controlled carefully to avoid causing obviously morphologic change to ER.[37] As expected, the same phenomena were observed with a

DOI: 10.1021/ja511273c
J. Am. Chem. Soc. 2015, 137, 436−444

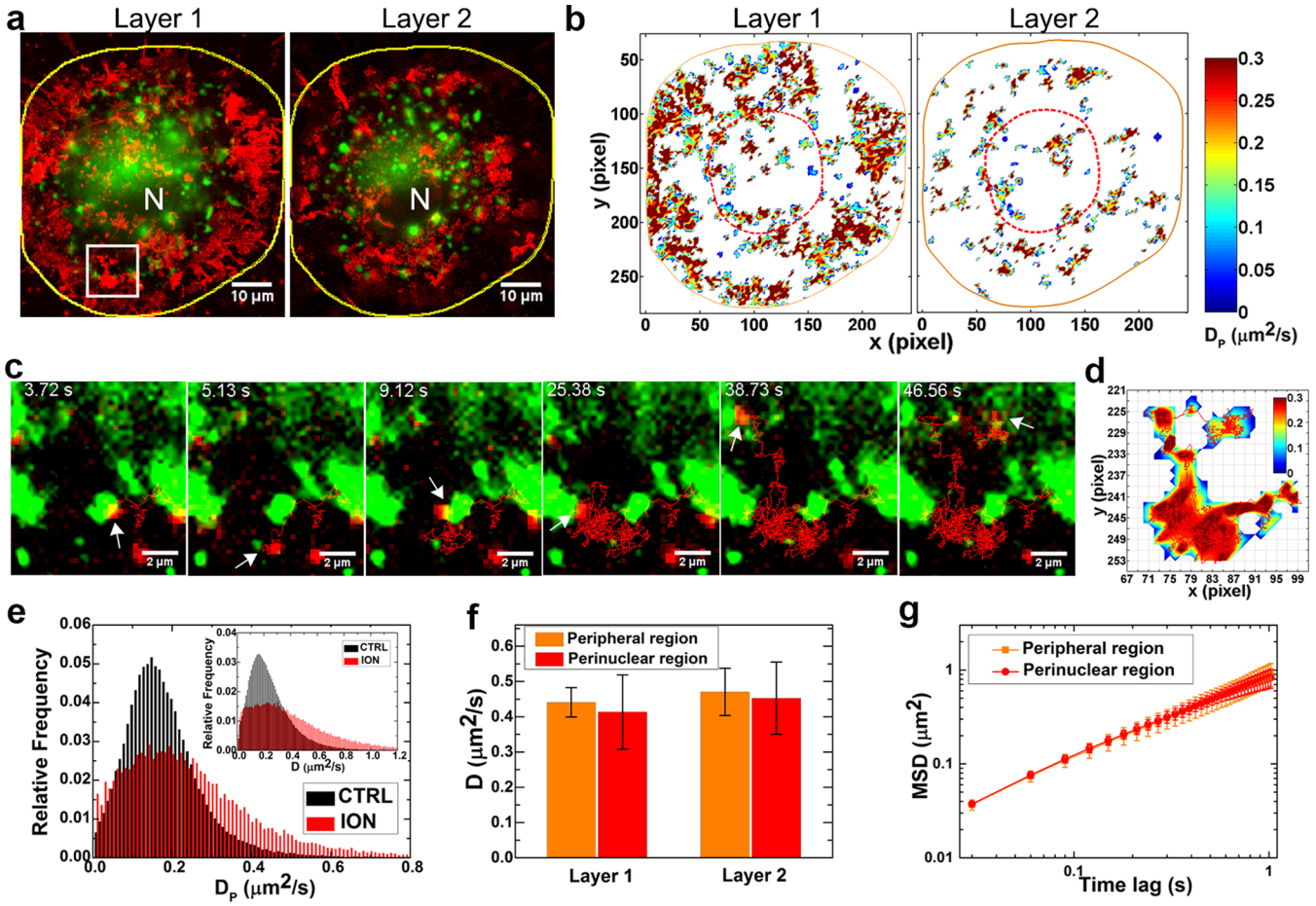

Figure 5. ER fragmentation relieves the diffusion restriction on QDs in ionomycin-treated cells. (a) Merged images of GFP-ER (green) with the superimposed image of 2000 consecutive frames of QDs (red) in the first and second layers. ERs are turned into fragments and surrounded by the QD tracks. The cell boundary is marked by a yellow line, and the nucleus position is denoted by N. (b) The corresponding diffusion maps in the two layers. (c) Image series of a QD trajectory (red) overlaid with GFP-ER (green) in the rectangular region marked in a. Arrows indicate the repeated collision between the QD and ER fragments. (d) Diffusion map plotted using the trajectory in (c) shows interconnected red areas corresponding to the interconnected ER-free areas. (e) Probability distributions of D_P in control (CTRL, 23 cells) and ionomycin-treated cells (ION, 24 cells). Inset, Probability distributions of D. (f) Average diffusion coefficient D in the peripheral and perinuclear regions separated by the red dash lines in (b) as determined with bright-field cell imaging. (g) Plots of average MSD in the two regions in the second layer. Images of five cells were used for the data in (f) and (g).

PC value of −0.41 ± 0.09 (Figures 4d and S8). In addition, we used QD-amine instead of QD-streptavidin and still obtained similar results (Figure 4d and Figure S9). Therefore, the compartmentalized diffusion of QD is indeed a result of barriers formed by ER tubules. ER tubules have a diameter of 60−100 nm,[38] which is more than twice larger than that of microtubules (25 nm), and are thus more apt to serve as physical barriers that deflect QDs. Note that the diffusion compartments observed in cytoplasm are much larger than those on cell membrane (<300 nm),[16−19] and one possible interpretation is that the larger intracellular compartments may provide enough space for the diffusion-mediated cellular processes of macromolecules, protein complexes, and vesicles.

To further study the influence of ER on QD diffusion, we treated cells with 1 μg/mL ionomycin for 10 min before imaging. In these cells, the original ER tubular and cisterna structures were turned into fragments (Figure 5a). The diffusion maps have more interconnected red areas of high diffusion rate (Figure 5b). A close look of a QD trajectory shows that the QD diffused over a wide range as long as it did not collide with an ER fragment on its path (Figure 5c and Movie S4), and the majority of its diffusion maps are interconnected red areas corresponding to the interconnected ER-free regions (Figure 5d). The distribution of D and D_P become wider than control (Figure 5e), suggesting an increase in diversity of the intracellular environment. In other words, the original ER structure makes the intracellular diffusion more uniform and controlled, which may be of relevance to its biological function. In the second layer, the previous barrier region disappeared. The QDs diffused throughout the cell except for the nucleus (Figure 5a). There is no obvious difference in diffusion coefficients or MSD curves between the peripheral and perinuclear areas in the ionomycin-treated cells (Figure 5f,g). Furthermore, we eliminated the possibility of the ionomycin (calcium ionophore) acting indirectly, by adding EGTA in advance to chelate the calcium in the culture medium, since the calcium is responsible for the ER fragmentation. The ER structure remained unchanged, and the results (Figure S10 and Figure 4d) were as same as those in Figure 4a−c. Note that, as one of the type III intermediate filament proteins, vimentin is also intensely distributed in the perinuclear region, overlapping with the ER cisterna.[32] But the possible role of

DOI: 10.1021/ja511273c
J. Am. Chem. Soc. 2015, 137, 436−444

vimentin in restricting the QD diffusion can be ruled out, because the treatment condition of ionomycin we used here was proved to have no obvious effect on the structure of vimentin filaments.[39,40]

Finally, to prove the compartmentalized diffusion is not from the nonspecific interaction between QDs and ER, we used 500 kD FITC-dextrans (the diameter is about 29 nm) as another kind of probe to repeat the experiments. The dextrans are noninteraction macromolecules that are widely used in intracellular diffusion studies.[1,29] The cells were transfected with RFP-ER, allowing us to simultaneously track the FITC-dextrans and RFP-ER movements. Although the brightness and photostability of this probe are not as good as QDs in SPT, based on the collected trajectories of FITC-dextrans, we still found the compartmentalized diffusion due to the ER tubules (Figure S11), just as expected. The PC value is -0.48 ± 0.06, comparable to that for QDs (Figure 4d). After ER fragmentation by ionomycin treatment, the compartmentalized diffusion also disappeared (Figure S12). These results suggest that the compartmentalized diffusion is general to intracellular macromolecules inside cells. And the reasonable mechanism of compartmentalized diffusion may be the following: the ER tubules not only act as physical barriers but also slow down the diffusion nearby, the latter of which could be through the increased viscosity as a result of approaching ER surface or entering the folded membranes of the ER which restricts locally the diffusion by reducing the available space. These factors act together to temporally confine the diffusing QDs or FITC-dextrans in the micron-scale domains defined by ER tubules.

■ CONCLUSIONS

In summary, we have introduced a novel method based on SPT to map the heterogeneous diffusion distribution of QDs in single cells and found a compartmentalized diffusion of QDs in cytoplasm, defined by ER tubules. The spatial resolution of the diffusion map, limited by the trajectory numbers for statistic analysis, may be improved by using higher frame rate and denser QDs. Thus, it is possible to use this method to further study finer intracellular organizations, composed of ER and various other organelles, for diffusion of protein-sized macromolecules.

The reason for the existence of differently shaped ER has not been fully elucidated.[34,38] Our observation of the ER-compartmentalized QD diffusion may provide clues about the functions of tubular ER. The compartments defined by ER tubules may serve to increase the probabilities of macromolecule bindings and biological reactions, through coconfined diffusion within them. Furthermore, the compartments subdivide the cytoplasm and produce a relatively organized environment for diffusion in cells that are crowded with complex macromolecules and diverse organelles, thus helping to regulate the diffusion-mediated cellular processes. "Form ever follows function", as said by Louis Sullivan, may be also true at the cellular level, at least for the ER tubule network.

■ EXPERIMENTAL SECTION

Reagent. QD streptavidin conjugate 655 nm (Q10123MP) and 525 nm (Q10143MP), and QD amine conjugate 655 nm (Q22021MP) were purchased from Invitrogen Corporation. All the three kinds of QDs have inner heavy PEG coating. QD carboxyl conjugate 655 nm was from Sigma-Aldrich (753866), without inner PEG coating. 500 kD FITC-dextran (D7136) was from Invitrogen Corporation. Nocodazole and cytochalasin D were from Sigma-Aldrich. Ionomycin was from Abcam Corporation. The living cell fluorescence labeling of organelles were done using the Cell Light Reagent from Invitrogen Corporation, including ER-GFP (C10590), ER-RFP(C10591), actin-GFP (C10506), tubulin-GFP (C10509), mitochondria-GFP (C10508), and Hoechst 33342 (nucleus stain, H3570). Ficoll 70 purchased from Amersham Corporation was prepared as 60 wt % stock solution and diluted to desired concentration with PBS before experiments. Other chemicals were from Sigma-Aldrich unless otherwise stated.

Cell Culture and Drug Treatment. Human lung carcinoma A549 cells (ATCC) were maintained in Dulbecco's modified Eagle medium (DMEM, GIBCO) with 10% fetal bovine serum (GIBCO) and 1% penicillin-streptomycin (GIBCO) incubated at 37 °C with 5% CO_2. Cells at the log phase were seeded in Petri dishes with poly-L-lysine-coated glass coverslips on the bottom the day before the experiments were conducted. To disrupt the microtubules or actin filaments, the cells were incubated with 20 μM nocodazole for 30 min or with 10 μM cytochalasin D for 10 min, respectively. To fragment the ER, the cells were incubated with 1 μg/mL ionomycin for 10 min. To chelate the calcium in the culture medium in case of the control experiments for ionomycin, the cells were pretreated with 2 mM EGTA in DMEM (calcium concentration 1.8 mM) for 10 min and then incubated with 1 ug/mL ionomycin in the presence of 2 mM EGTA for 10 min. The drugs were maintained in the medium throughout the experiments.

QD Internalization in Living Cells. The QDs to be tracked were loaded into live cells via a pinocytic process.[25] The QDs were mixed at a concentration of 0.5−5 nM with a hypertonic solution (Influx-pinocytic cell-loading reagent (I-14402), Invitrogen). Cells were incubated for 10 min at 37 °C in the solution, allowing the material to be carried into the cells via pinocytic vesicles. Then the cells were transferred to a hypotonic medium for 2 min, which resulted in the release of trapped QDs from the pinocytic vesicles within the cells. The cells were then left in complete DMEM at 37 °C with 5% CO_2 to recover for 10 min before imaging. The osmotic lysis of pinocytic vesicles in the hypotonic solution did not alter the viability of cells and did not result in lysosomal enzyme release. The serum-free, phenol red-free DMEM was used as the imaging medium. The FITC-dextrans were loaded using the same method, at a concentration of 0.2−0.5 mg/mL.

Fluorescence Microscopy. Wide-field and highly inclined and laminated optical sheet (HILO) imaging for SPT was performed using an inverted Olympus IX70 microscope equipped with a 60× oil TIRF objective (1.45 N.A., Olympus) and back-illuminated EMCCD camera (DU-897, Andor Technology). The microscope was equipped with a CO_2 incubation system (TOKAI HIT), and the whole course of live cell imaging was performed at 37 °C with 5% CO_2 condition, which is crucial for maintaining the physiological environment of cells. DIC optics (Olympus) was used to obtain cell body images before and after the fluorescence imaging. The cells in mitosis phase were eliminated. In the case of SPT in PBS or Ficoll 70, the imaging focal plane was selected at 10−20 μm above the glass surface to avoid the possible influence by the surface and reduce the background fluorescence from QDs on the surface.

At the excitation path, three lasers of different wavelengths were used: a 405 nm laser (OBIS 405−100 mW, Coherent) for imaging Hoechst, a 488 nm laser (Sapphire 488−200cW, Coherent) for imaging GFP, QD525, and FITC-dextran, and a 561 nm laser (Sapphire 561−200cW, Coherent) for imaging RFP and QD655. Mechanical shutters (Uniblitz LS6T2, Vincent Associates) were used to control the on−off state of these lasers. The laser intensities were controlled by the laser power supplies. All laser beams were combined by dichroic mirrors and coupled into an optical fiber (Oz Optics). The output light from the optical fiber was focused at the back focal plane of the objective.

In the emission path, fluorescence emission was collected through the objective and separated from the excitation lasers using a triple-band dichroic mirror and a triple-band emit filter. In the case of two-color imaging, a dual-channel simultaneous-imaging system (DV2, Photometrics) was used to image QD525 and QD655, GFP and QD655, or FITC-dextran and RFP, on an EMCCD. The spectral

DOI: 10.1021/ja511273c
J. Am. Chem. Soc. 2015, 137, 436−444

windows of the captured images were defined by a dichroic filter and two emission filters in the image splitter (T565lpxr, ET525/50m for QD525, GFP and FITC-dextran, D655/40m for QD655 and RFP, Chroma). The two subimages were calibrated by imaging fluorescent beads (Invitrogen) that have an emission spectrum covering the two spectral windows.

Images of QDs in living cells or Ficoll 70 (10−60 wt %) were acquired at 33 Hz for a total of 2000 frames (1 min). In order to track the rapid QDs in PBS and in Ficoll 70 (5 wt %), images were acquired at 100 Hz for a total 6000 frames of a subarea of the EMCCD chip of 128 × 512 pixel^2.

Single-Particle Tracking. Analysis of the acquired image series was performed as described previously,[28] by using the ImageJ plugin Particle Tracker.[41] For each frame, individual QDs were detected and localized by adjusting parameters for radius, cutoff, and percentile. The parameter of percentile was adjusted to capture the greatest number of QDs that were visible clearly. The parameter for cutoff was set to exclude the possibly few aggregations as well as the blurred QDs which were partially out of focus. Localization accuracy of the system was about 30 nm, as determined by imaging fixed QDs under the same imaging conditions as that for cells. The parameters of linking range and displacement were adjusted to link the detected particles between frames. In case of SPT in cells, the linking range was set to 3 to bridge over short QD blinking events (no more than 3 frames). The displacement was chosen not <2 pixels to detect QDs diffusing as fast as 2.34 μm^2/s theoretically, far beyond the actual mean D of 0.3 μm^2/s. The limitation of the detected diffusion rate was estimated by the following equation: $D = L^2/4\Delta t$, where L is 0.53 μm, and Δt is 0.03 s. For the FITC-dextran, the same method was used. Compared with QDs, the FITC-dextran had a lower intensity and might be photobleached during imaging, causing low-quality images in SPT. In case of SPT in PBS and in Ficoll 70 (5 wt %), we increased the displacement to track the rapid QDs and decreased the linking range to avoid wrong linking.

All the linking parameters were optimized repeatedly, and the linking steps were checked optically for possible inappropriate linking adjustments. All individual trajectories visually detected were included in our analysis database, and trajectories longer than 30 frames were selected for further analysis.

Data Analysis. All data analyses were performed using user-defined program in Matlab. The trajectories were all filtered twice before the following MSD analysis: (1) intensities filter was used to remove the potential QD aggregates whose intensities were beyond 1.5 times that of the mean intensity of all the QDs, and the potential out-of-focus QDs whose intensities were below 0.5 times that of the mean intensity; (2) fixation filter to remove the fixed QDs with displacements <100 nm, and the length was estimate by using the QDs fixed on glass in 1 min imaging. In the case of FITC-dextran, the same procedure and parameters were applied.

The local MSD analysis was used to select and analyze the diffusive motion of the QD trajectories containing occasional immobilization. For each point along the trajectory a local MSD is computed, considering only the neighboring 30 trajectory points. It was calculated by

$$\mathrm{MSD}(n\tau) = \frac{1}{30-n}\sum_{i=-15}^{15}\begin{bmatrix}(x((i+n)\tau) - x(i\tau))^2 \\ +(y((i+n)\tau) - y(i\tau))^2\end{bmatrix} \quad (1)$$

where τ is the acquisition time, and n = 1−10. Note that the effect of QD blinking was considered in the calculation. Then MSD was fitted by the power law $\mathrm{MSD}(n\tau) = A\cdot(n\tau)^{\alpha}$.

The exponent α indicates the nonlinear relationship of MSD with time, which carries information about the local motion modes:[12,28] $\alpha \approx 1$ being free Brownian motion (e.g., pure random walk or free diffusion), $\alpha < 1$ subdiffusion (e.g., diffusion within a confined area), $\alpha > 1$ superdiffusion (e.g., diffusion overlaid with deterministic motion), and $\alpha \approx 2$ directed motion. Similarly, the diffusion rate D of the point is determined by fitting the 3 initial points of the local MSD curve with $\mathrm{MSD}(n\tau) = 4D\cdot n\tau + c$, which is a commonly used standard in SPT. This fit is repeated for each point along the trajectory, resulting in time series for the parameter α and D. The mean D for the single cell is the average from all the local values of the points in the cell.

Note that the local and time-resolved parameter α has additional noise because of the smaller sample. In this work, we aim to select the diffusion motion and discard the immobility. To obtain the criterion of selection, the QDs fixed on glass were analyzed as immobility control with $\alpha < 0.5$, and the QDs diffusing in Ficoll 70 were as Brownian motion control with $0.5 < \alpha < 1.5$. The α distribution of QDs in cells showed a combination of immobility and Brownian motion, so we finally selected the segments of trajectories of which the consecutive points with the criteria $0.5 < \alpha < 1.5$ were equal to or longer than 5 frames. Only the segments belonging to diffusion were used in the statistics of diffusion coefficient and in plotting the diffusion map.

To test the effectiveness of the exponent α method of identifying immobilized events, the positional accuracy method was then used. The positional accuracy σ was 30 nm, leading to a constant offset in MSD of 0.0036 μm^2/s ($4\sigma^2$). If the local MSD value of consecutive points (>5 frames) is close to this value, the segment consisting of these points could be considered immobile.

In the case of global MSD analysis, the whole trajectory of one specific QD was used to generate the MSD plot, which was used to analyze the global exponent α of all the trajectories.

Diffusion Map Plotting. The plotting was performed using custom-written program in Matlab. Only the selected segments in diffusive motion mentioned above were used to plot the diffusion map. First, the square grids in pixels was generated to divided area covered by the cell. Each grid node served as a point in the diffusion map, and the grid size corresponded to the spatial resolution of the diffusion map. The point value was equal to its local diffusion coefficient D_P. Second, the parts of all the segments within a distance threshold to the grid node were picked out. Third, the ensemble-averaged MSD curve was calculated using the parts of segments. Only when the first three points of MSD curve were calculated using more than five samples for each point, the ensemble-averaged MSD curve was valid. Fourthly, the following local diffusion coefficient D_P was determined by linearly fitting the initial three points of the MSD curve. The final grid size and distance threshold were chosen to be 2 pixels (533 nm) and 1.5 pixels (400 nm), respectively, by considering the QD diffusion rate and sample size of experiments. The average lag time of segments covered by the distance threshold of 1.5 pixels was about 0.16 s, which was estimated conservatively by $\Delta t = L^2/4D$, where L was selected as 0.4 μm (radius of the circle), and D was 0.25 μm^2/s. Finally, the contour map of D_P was plotted in Matlab, with a built-in smoothing process. The effective spatial resolution of the diffusion maps here was 2 pixels. In the case of FITC-dextrans, the same method was used, except both the final grid size and distance threshold were 2 pixels (533 nm) to adapt to the fast diffusion rate of FITC-dextrans.

PC Calculating. The PC calculating was performed using the built-in function in Matlab. For the two variables, the D_P of diffusion map (X) and the ER fluorescence intensity (Y), their linear correlation was measured by the PC:

$$\mathrm{PC} = \frac{\sum_i (X_i - \bar{X})(Y_i - \bar{Y})}{\sqrt{\sum_i (X_i - \bar{X})^2}\sqrt{\sum_i (Y_i - \bar{Y})^2}} \quad (2)$$

Since the values of D_P are unavailable in blank areas of the diffusion map, blank areas would be excluded in the PC calculation if they were encountered. Considering the continuous reorganization of the ER network, the middle one in the ER image series of 1 min was used for the calculating. As a control for the evaluation of PC, the randomization of the ER fluorescence image was used, then the calculated PC was around zero.

Image Processing. All image processing was performed using ImageJ software, including producing the movies, aligning and merging of two-color images or stacks, magnifying the images, and measuring the intensity along marked lines. The boundaries of cells were manually selected in DIC images.

DOI: 10.1021/ja511273c
J. Am. Chem. Soc. 2015, 137, 436−444

■ ASSOCIATED CONTENT

Supporting Information

Diffusion coefficients for different QDs in Ficoll 70 and in cells with different treatments (Table S1). Diffusion coefficient verse viscosity (Figure S1), comparison of diffusion rates (Figure S2), amount of internalized QDs (Figure S3), positional accuracy method for immobile events (Figure S4), diffusion map without smoothing process (Figure S5), merged image of mitochondria and QDs (Figure S6), effect of drugs for depolymerizing cytoskeletons (Figure S7), compartmentalized diffusion of QD-streptavidin in NOC-treated cells (Figure S8), compartmentalized diffusion of QD-amine in control cells (Figure S9), compartmentalized diffusion of QD-streptavidin in EGTA and ionomycin-treated cells (Figure S10), compartmentalized diffusion of FITC-dextrans in control cells (Figure S11), and the diffusion of FITC-dextrans in ionomycin-treated cells (Figure S12). This material is available free of charge via the Internet at http://pubs.acs.org.

Web-Enhanced Features

Four WEOs are available in the HTML version of the paper. Movies of QD diffusion in single cell (Movie S1) and in different layers of a single cell (Movie S2) and QD movements with the intact ER (Movie S3) and fragmented ER (Movie S4).

■ AUTHOR INFORMATION

Corresponding Author

*pywang@aphy.iphy.ac.cn

Notes

The authors declare no competing financial interest.

■ ACKNOWLEDGMENTS

This research was supported by the National Natural Science Foundation of China (11304372, 11204363, 11274374) and the National Basic Research Program of China (973 Program) (Grant 2013CB837200).

■ REFERENCES

(1) Luby-Phelps, K. *Int. Rev. Cytol.* **2000**, *192*, 189.
(2) Dix, J. A.; Verkman, A. S. *Annu. Rev. Biophys* **2008**, *37*, 247.
(3) Zhou, H. X.; Rivas, G.; Minton, A. P. *Annu. Rev. Biophys* **2008**, *37*, 375.
(4) Kuimova, M. K.; Yahioglu, G.; Levitt, J. A.; Suhling, K. *J. Am. Chem. Soc.* **2008**, *130*, 6672.
(5) Peng, X.; Yang, Z.; Wang, J.; Fan, J.; He, Y.; Song, F.; Wang, B.; Sun, S.; Qu, J.; Qi, J.; Yan, M. *J. Am. Chem. Soc.* **2011**, *133*, 6626.
(6) Verkman, A. S. *Trends Biochem. Sci.* **2002**, *27*, 27.
(7) Kalwarczyk, T.; Ziebacz, N.; Bielejewska, A.; Zaboklicka, E.; Koynov, K.; Szymanski, J.; Wilk, A.; Patkowski, A.; Gapinski, J.; Butt, H. J.; Holyst, R. *Nano Lett.* **2011**, *11*, 2157.
(8) Lidke, D. S.; Wilson, B. S. *Trends Cell Biol.* **2009**, *19*, 566.
(9) Ramadurai, S.; Holt, A.; Krasnikov, V.; van den Bogaart, G.; Killian, J. A.; Poolman, B. *J. Am. Chem. Soc.* **2009**, *131*, 12650.
(10) Luby-Phelps, K.; Taylor, D. L.; Lanni, F. *J. Cell Biol.* **1986**, *102*, 2015.
(11) Luby-Phelps, K. *Mol. Biol. Cell* **2013**, *24*, 2593.
(12) Saxton, M. J.; Jacobson, K. *Annu. Rev. Biophys. Biomol. Struct.* **1997**, *26*, 373.
(13) Brameshuber, M.; Schutz, G. J. *Nat. Methods* **2008**, *5*, 133.
(14) Andrews, N. L.; Lidke, K. A.; Pfeiffer, J. R.; Burns, A. R.; Wilson, B. S.; Oliver, J. M.; Lidke, D. S. *Nat. Cell Biol.* **2008**, *10*, 955.
(15) Jaqaman, K.; Kuwata, H.; Touret, N.; Collins, R.; Trimble, W. S.; Danuser, G.; Grinstein, S. *Cell* **2011**, *146*, 593.
(16) Clausen, M. P.; Lagerholm, B. C. *Nano Lett.* **2013**, *13*, 2332.
(17) Jacobson, K.; Mouritsen, O. G.; Anderson, R. G. W. *Nat. Cell Biol.* **2007**, *9*, 7.
(18) Pinaud, F.; Michalet, X.; Iyer, G.; Margeat, E.; Moore, H. P.; Weiss, S. *Traffic* **2009**, *10*, 691.
(19) Kusumi, A.; Fujiwara, T. K.; Chadda, R.; Xie, M.; Tsunoyama, T. A.; Kalay, Z.; Kasai, R. S.; Suzuki, K. G. N. *Annu. Rev. Cell Dev. Biol.* **2012**, *28*, 215.
(20) Wirtz, D. *Annu. Rev. Biophys.* **2009**, *38*, 301.
(21) Michalet, X.; Pinaud, F. F.; Bentolila, L. A.; Tsay, J. M.; Doose, S.; Li, J. J.; Sundaresan, G.; Wu, A. M.; Gambhir, S. S.; Weiss, S. *Science* **2005**, *307*, 538.
(22) Pinaud, F.; Clarke, S.; Sittner, A.; Dahan, M. *Nat. Methods* **2010**, *7*, 275.
(23) Delehanty, J. B.; Mattoussi, H.; Medintz, I. L. *Anal. Bioanal. Chem.* **2009**, *393*, 1091.
(24) Summers, H. D.; Rees, P.; Holton, M. D.; Brown, M. R.; Chappell, S. C.; Smith, P. J.; Errington, R. J. *Nat. Nanotechnol* **2011**, *6*, 170.
(25) Okada, C. Y.; Rechsteiner, M. *Cell* **1982**, *29*, 33.
(26) Dauty, E.; Verkman, A. S. *J. Mol. Recognit.* **2004**, *17*, 441.
(27) Lisse, D.; Richter, C. P.; Drees, C.; Birkholz, O.; You, C. J.; Rampazzo, E.; Piehler, J. *Nano Lett.* **2014**, *14*, 2189.
(28) Li, H.; Duan, Z. W.; Xie, P.; Liu, Y. R.; Wang, W. C.; Dou, S. X.; Wang, P. Y. *PLoS One* **2012**, *7*, e45465.
(29) Seksek, O.; Biwersi, J.; Verkman, A. S. *J. Cell Biol.* **1997**, *138*, 131.
(30) Wachsmuth, M.; Waldeck, W.; Langowski, J. *J. Mol. Biol.* **2000**, *298*, 677.
(31) Murase, K.; Fujiwara, T.; Umemura, Y.; Suzuki, K.; Iino, R.; Yamashita, H.; Saito, M.; Murakoshi, H.; Ritchie, K.; Kusumi, A. *Biophys. J.* **2004**, *86*, 4075.
(32) Provance, D. W.; Mcdowall, A.; Marko, M.; Lubyphelps, K. *J. Cell Sci.* **1993**, *106*, 565.
(33) Subramanian, K.; Meyer, T. *Cell* **1997**, *89*, 963.
(34) English, A. R.; Voeltz, G. K. *Cold Spring Harbor Perspect. Biol.* **2013**, *5*, a013227.
(35) Manders, E. M.; Stap, J.; Brakenhoff, G. J.; van Driel, R.; Aten, J. A. *J. Cell Sci.* **1992**, *103* (Pt 3), 857.
(36) Waterman-Storer, C. M.; Salmon, E. D. *Curr. Biol.* **1998**, *8*, 798.
(37) Lu, L.; Ladinsky, M. S.; Kirchhausen, T. *Mol. Biol. Cell* **2009**, *20*, 3471.
(38) Park, S. H.; Blackstone, C. *EMBO Rep.* **2010**, *11*, 515.
(39) Asaga, H.; Yamada, M.; Senshu, T. *Biochem. Biophys. Res. Commun.* **1998**, *243*, 641.
(40) Oguri, T.; Inoko, A.; Shima, H.; Izawa, I.; Arimura, N.; Yamaguchi, T.; Inagaki, N.; Kaibuchi, K.; Kikuchi, K.; Inagaki, M. *Genes Cells* **2006**, *11*, 531.
(41) Sbalzarini, I. F.; Koumoutsakos, P. *J. Struct. Biol.* **2005**, *151*, 182.

DOI: 10.1021/ja511273c
J. Am. Chem. Soc. 2015, 137, 436−444